

Article

InSAR Observation and Numerical Modeling of the Earth-Dam Displacement of Shuibuya Dam (China)

Wei Zhou ¹, Shaolin Li ^{1,2}, Zhiwei Zhou ^{3,*} and Xiaolin Chang ¹

¹ State Key Laboratory of Water Resources and Hydropower Engineering Science, Wuhan University, Wuhan 430072, China; zw_mxx@163.com (W.Z.); shaolin@whu.edu.cn (S.L.); changxl@whu.edu.cn (X.C.)

² Changjiang Institute of Survey, Planning, Design and Research, Wuhan 430010, China

³ Global Navigation Satellite System Research Centre, Wuhan University, Wuhan 430079, China

* Correspondence: zhiwei8848@gmail.com; Tel.: +86-27-6877-8240; Fax: +86-27-6877-8971

Academic Editors: Zhenhong Li, Roberto Tomas, Zhong Lu and Prasad S. Thenkabail

Received: 30 June 2016; Accepted: 13 October 2016; Published: 23 October 2016

Abstract: How to accurately determine the mechanical parameters of rockfill is one of the key issues of concrete-face rockfill dams. Parameter back-analysis using internal or external monitoring data has been proven to be an efficient way to solve this problem. However, traditional internal or external monitoring methods have limitations in efficiency and long-term monitoring. In this paper, the displacement of the Shuibuya concrete-face rockfill dam is monitored by the space-borne Interferometric Synthetic Aperture Radar (InSAR) time series method. Using the InSAR results and the finite element method, the back-analysis of the mechanical parameters of the rockfill dam is investigated, and the back-analysis results of InSAR and levelling are compared. A high correlation of 0.99 for the displacement results generated from InSAR and the levelling offers good agreement between the two methods. The agreement provides confidence that the external InSAR monitoring measurement allows producing a reliable back-analysis and captures the displacement properties of the dam. Based on the identified parameters from the InSAR results, the dam displacement is predicted. The prediction of the maximum settlement of the dam is 2.332 m by the end of 2020, according to the dam displacement characteristics, which agrees well with the results derived from the recorded internal monitoring data. Therefore, the external monitoring results from the InSAR observation can be used as a supplement for traditional monitoring methods to analyse the parameters of the dam.

Keywords: Interferometric Synthetic Aperture Radar (InSAR) time series; Concrete-Face Rockfill Dam (CFRD); numerical modelling; finite element method; back-analysis

1. Introduction

In the stability and security analysis of the concrete-face rockfill dams (CFRDs), the physical parameters of the rockfill are pre-requisite for settlement prediction. Because of the complexity of the dam characteristics, the material properties are influenced by the loading, load size, stress path and other factors in the engineering project. Currently, engineering analogy, expert experience and experimentation are used to determine the material parameters of the rockfill. However, engineering analogies and expert experience require users who have rich experience in engineering and detailed engineering data. Lots of subjective factors are contained in the results. Due to the scale effect, sample disturbance and the impact of random sampling, it is difficult to guarantee the representation of the experiment results [1,2]. Moreover, even though the accurate design parameters of the rockfill are obtained by experiment, the values are greatly different from the actual engineering parameters due to the influence of the construction process, construction technology, construction quality, the external

environment and other factors. Therefore, the stress–strain analysis, operational behaviour analysis and safety evaluation based on the experimental parameters cause great error in CFRDs.

Parameter back-analysis using the internal or external monitoring data has proven to be an efficient way to identify the physical parameters of the rockfill [3,4]. Based on the identified parameters, the stability and security analysis of the CFRDs can be investigated using the finite element method (FEM) [5]. The internal monitoring methods include tension wire alignment and hydraulic overflow settlement gauges [6–8]. However, these internal monitoring methods do not meet the safety monitoring requirements of large dams in terms of efficiency and long-term observations because of their low coverage and durability, and labour-intensive monitoring needs. The internal monitoring data, the optimization algorithm and the artificial neural network are used in traditional back-analysis to identify the parameters of the rockfill dam [3,9–11]. Generally, external monitoring methods include levelling or Global Position System (GPS) measurement, but they are rarely used in back-analysis. Traditional back-analysis requires many training samples when using the artificial neural network and is time-consuming and inefficient. To overcome these disadvantages, a response surface method (RSM) may be applied during the processing [4].

In the past two years, interferometric synthetic aperture radar (InSAR) has proven to be a powerful tool to measure the Earth's surface movements. Few studies have focused on using InSAR to map the displacement of dam bodies and/or reservoir slopes [12–15], and back-analysis in high CFRDs based on InSAR observations has not been performed. In this study, we aim to use the space-borne InSAR time series results of Shuibuya (SBY), the RSM and the FEM to investigate the physical parameters of the rockfill of the SBY Dam and to predict its long-term displacement of the dam. The numerical results calculated using the back-analysis model parameter set based on the InSAR results are compared with the levelling monitoring data.

This paper is structured as follows: Section 2 presents the general description of the SBY Dam. Section 3 presents the SAR data, a short description of InSAR time series processing and the InSAR time series results. The constitutive model, back-analysis method, identified parameters set, validation, stress and displacement analysis are given in Section 4. Finally, the discussions and conclusions are presented in Sections 5 and 6.

2. Study Area

Located on the middle stream of the Qingjiang River in the Enshi Autonomous Prefecture, Hubei Province, China, the SBY CFRD (110.3377°N, 30.4374°E) is approximately 117 km upstream of the city of Enshi and 92 km from the downstream Geheyan Hydropower Plant (Figure 1). The height of the SBY CFRD is up to 233.5 m, and the crest length is 675 m. The normal water level of the reservoir is 400 m above sea level, and the maximum water storage of the reservoir is approximately $4.59 \times 10^9 \text{ m}^3$. The SBY Dam has four generators in its underground power plant, with a total electric generating capacity of 1840 MW. It is a typical concrete-face rockfill dam, and its body is composed of six material zones: arbitrary fill material, bedding material, transition material, primary rockfill, secondary rockfill and downstream rockfill (Figure 2a). The upstream and downstream of the dam has the same slope of 1:1.4. The construction began in October 2002 and can be divided into three reference periods:

- I Dam construction period (before October 2006).
- II The first reservoir filling period (October 2006–September 2007, when the water level was between 205.06 m above sea level and 389.61 m).
- III Operation period (after September 2007).

Because of the significance of the project, an improved and detailed settlement monitoring system was implemented for the SBY CFRD, including eleven levelling monitoring stations distributed downstream of the dam. The eleven monitoring stations (WS1 to WS11) were established at elevations of 235 m, 265 m, 300 m, 335 m, and 370 m to monitor the settlement of the downstream dam surface (as shown in Figure 2b).

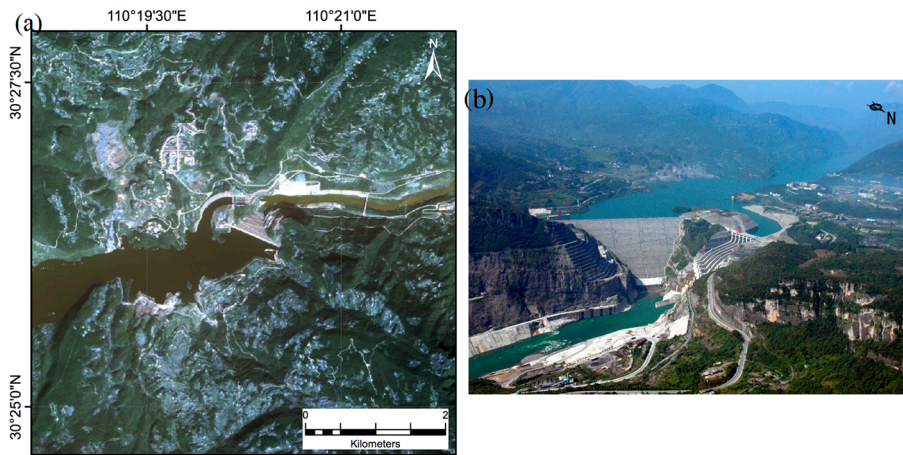


Figure 1. The location of the study area and the Shuibuya Reservoir: (a) The location of the Shuibuya Reservoir (red triangle); and (b) View of the Shuibuya concrete-face rockfill dam (CFRD). This figure is adapted from [16].

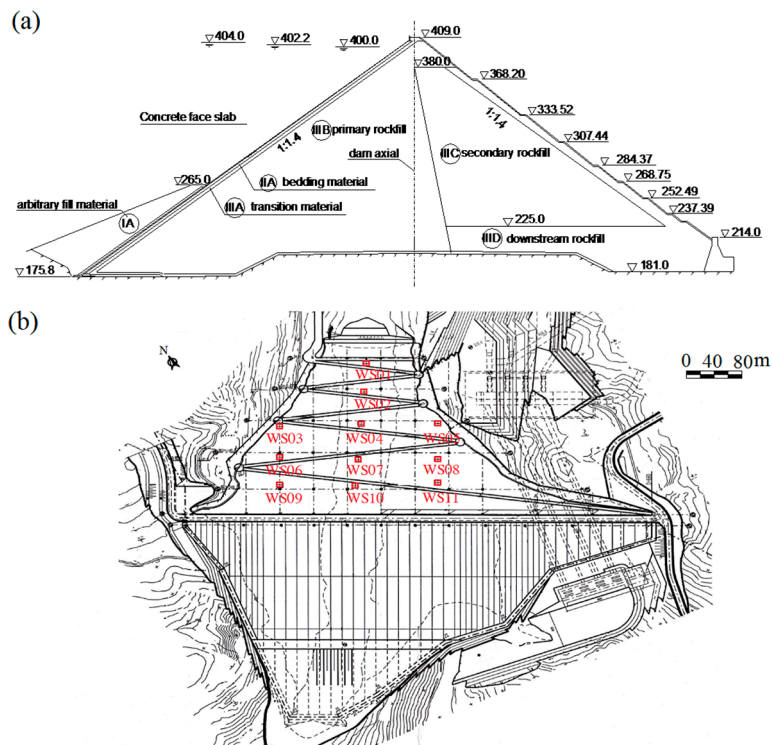


Figure 2. Typical zoning and layout of the exterior settlement monitoring system of the Shuibuya CFRD: (a) The six material zones; and (b) The eleven external settlement monitoring stations. This figure is adapted from [16].

3. InSAR Data Analysis and Results

A detailed InSAR data processing steps and analysis about the SBY dam is performed in our previously paper [16]. Here, we present a short description of the InSAR processing and related results. Twenty-one ascending ALOS-1 PALSAR L-band (~23.6 cm wavelength) images acquired from the Japan Aerospace Exploration Agency were used to map the displacement of the SBY Dam. The ALOS-1 satellite was launched in January 2006 and terminated in April 2011. Only images from 28 February 2007 to 11 March 2011 were processed, representing the period after completion of the dam (Figure 3).

In the single-imaging mode, the resolution of the images is approximately 4.7 m in the slant range and 4.5 m in the azimuth direction. The incidence angle is approximately 38.7° . There are many archived ESA Envisat ASAR C-band (~ 5.6 cm) images, however the resolution is too low (~ 20 m). Considering the scale of the dam, ASAR data is not suitable for this study. Although the resolution of the TerraSAR-X and Cosmo-SkyMed X-band (~ 3 cm) images are much higher (up to 1 m), there is very little archived data in this area at present. That means these data are not suitable for the InSAR time series analysis.

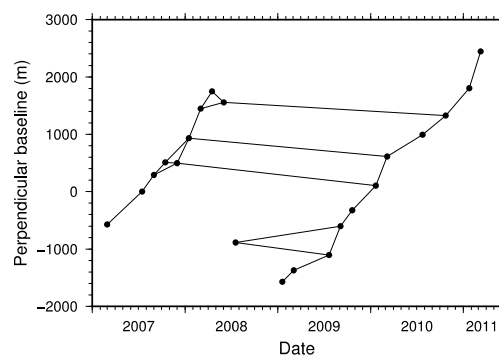


Figure 3. Interferogram distribution in terms of the spatial and temporal baseline, adapted from [16]. Each black circle represents one SAR image and the black solid line between two circles represents one interferogram.

The GAMMA processing package was used to generate single look complex (SLC) products from the set of raw SAR images [17]. All SLC images were co-registered to a chosen master image (2 June 2008) to match the dataset to its later interferogram generation. Next, an area of approximately $5 \text{ km} \times 5 \text{ km}$ ($1000 \text{ pixels} \times 1000 \text{ pixels}$) centred on the SBY Dam was cropped from the original $70 \text{ km} \times 70 \text{ km}$ SLC images (Figure 4a). All possible interferograms were generated with a spatial baseline below 2000 m and temporal baselines below 30 months. Then, interferograms were investigated visually, and only interferograms with a valid phase and coverage greater than 70% were kept for later InSAR time series analysis. Finally, 26 interconnected interferograms were selected (Figure 3). Topographic fringes of each interferogram was subtracted by using the 1-arc second (~ 30 m) Shuttle Radar Topography Mission (SRTM) Digital Elevation Model (DEM) [18], and the MCF algorithm was used to unwrap the phase [19]. Given the image resolution and the scale of the SBY Dam, multi-looking processing was not performed in this study.

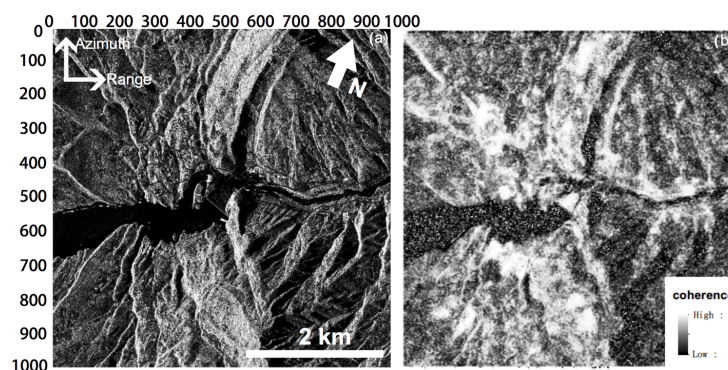


Figure 4. The cropped study area and the average coherence map in radar geometry (not geocoded): (a) The amplitude image of the study area; and (b) The average coherence map, where white indicates pixels with strong coherence and black indicates pixels with low or no coherence. This figure is quoted from [16].

Generally, the unwrapped phase consists of five terms: displacement signal, inaccurate orbital information, topographic error, atmospheric propagation delays (atmospheric phase screen, APS), and noise [20]. There are various approaches have been developed to reduce the latter four terms based on multi-interferogram analysis [21–25]. In this study, the InSAR Time Series with the Atmospheric Estimation Model (InSAR TS + AEM, [26]) is used to perform the time series analysis, which is based on the Small Baseline Subset algorithm (SBAS) (e.g., [22]). The temporal or intermittent coherent pixels strategy was applied to increase the density and distribution of stable pixel [27,28]. The Figure 4b shows the average coherence of the study area.

Because the study area is approximately 5 km × 5 km, a linear plane across the entire interferogram is sufficiently accurate to remove the orbital error [20]. For a given set of unwrapped interferograms, topographic error signals can be separated because they are proportional to the perpendicular baselines [20]. Therefore, the orbital and topographic error can be estimated and individually removed from the unwrapped phase. Taking into account the spatial structure of atmospheric effects (only correlated in space) (e.g., the power-law process [29,30]), the APS can be estimated using a temporary linear velocity (TLV) model and can be distinguished from non-linear surface motion, more details can be found from [26]. The algorithm was applied iteratively until convergence was achieved [26,31]. A small area (500 m × 500 m) in the village was assumed to be stable during the InSAR observations and was therefore selected as the reference site for the InSAR time series analysis (Figure 4a). For a given pixel, the LOS displacement contains three displacement components in east, north and up direction. It is a function of incidence angle and above three components:

$$d_{los} = \cos\alpha \sin\theta d_e - \sin\alpha \cos\theta d_n - \cos\theta d_u \quad (1)$$

where d_e , d_n , d_u , are displacements in east, north and up directions respectively, α is the azimuth of the satellite heading (positive clockwise from the north) and θ is the radar incidence angle.

In this study, we assume that the horizontal components are negligible. Assuming this, the vertical component can then be converted from d_{los} using the local incidence angle: $d_u = -d_{los}/\cos\theta$. The LOS mean velocity and LOS time series were both converted into vertical direction measurements (Figure 5a). Eleven points at the same locations as the eleven WS stations of the dam were used to investigate the accuracy of the InSAR measurements. These eleven locations were carefully selected by cross-reference of the optical image, SAR amplitude image, and the ground monitoring locations. Finally, a high correlation of 0.9 and an RMS of 1.57 cm/year provided confidence that InSAR can produce reliable monitoring results (Figure 5b).

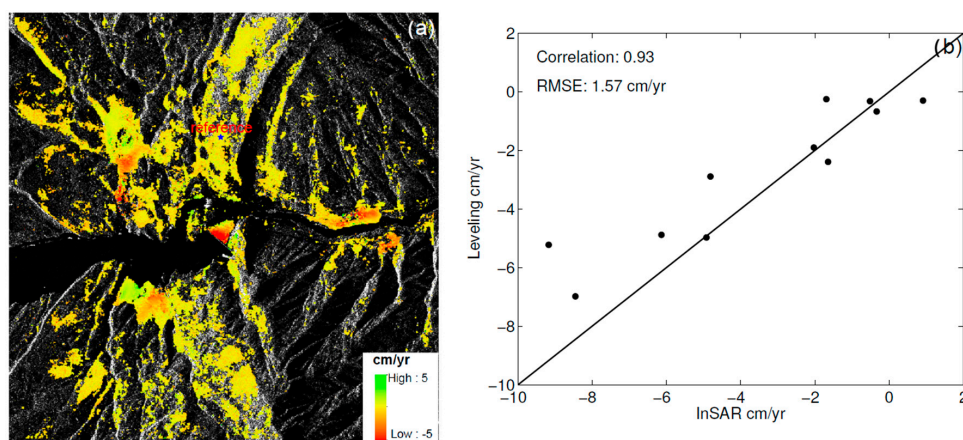


Figure 5. InSAR Vertical displacement velocity of the study area in radar geometry (not geocoded), and comparisons between the levelling: (a) The vertical displacement velocity, the blue star presents the reference location; and (b) The comparisons between InSAR and levelling measurements, black lines is a 1:1 line. This figure is adapted from [16].

4. Mechanical Parameter Back-Analysis Using the FEM and InSAR Results

4.1. Mechanical Parameters Back-Analysis Method

Rockfill model parameters back-analysis is used to find one group of parameters that make the calculated and observed displacement correspond. This process includes the following steps (shown in Figure 6):

- 1 Build the objective function using the InSAR results, as Equation (2). Equation (2) presents the InSAR results of i th monitoring point.
- 2 Perform the strain-stress analysis using the FEM (see Section 4.1.1) and the calculation of the RSM as defined in Section 4.1.2. Using the RSM, simulate the relationship between the parameter set and the displacement of each monitoring point.
- 3 Find the optimal parameter set of the objective function using the modified genetic algorithm (GA) introduced in Section 4.1.3. The optimal parameter set is a combination of the material parameters that minimize the objective function. During the process of searching, these RSM are used to replace the FEM to calculate the fitness of all the measurement points.

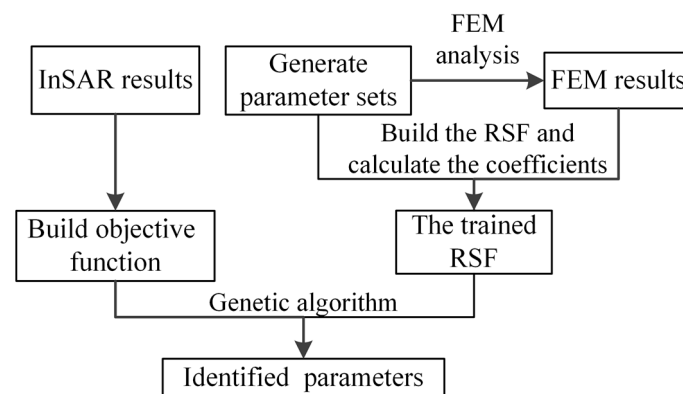


Figure 6. The flow chart of the parameter back-analysis.

The 2-norm of the difference between the calculated and observed displacement at the measuring points is used to build the objective function.

$$f(\lambda_1, \lambda_2, \dots, \lambda_n) = \left[\frac{1}{n} \sum_{i=1}^n \left(\frac{u_i - u_i^*}{u_i^*} \right)^2 \right]^{0.5} \quad (2)$$

where $(\lambda_1, \lambda_2, \dots, \lambda_n)$ is a group of constitutive parameters to be identified, u_i is the calculated displacement at the monitoring point i , u_i^* is the corresponding measured displacement and n is the number of monitoring points used in the back-analysis.

4.1.1. The FEM Model and the Constitutive Model

To further extend the investigation of the settlement determined by the InSAR analysis, we used the finite element method to conduct mechanical parameter back-analysis and strain-stress analysis, which allowed us to account for all geological and geophysical information available for the considered area. As a numerical technique, the FEM is used to find approximate solutions to boundary value problems consisting of partial differential equations and boundary conditions. The FEM subdivides a large problem into smaller, simpler, parts, called finite elements. The simple equations that model these finite elements are then assembled into a larger system of equations that models the entire problem. Then, the FEM uses variational methods from the calculus of variations to approximate a solution by minimizing an associated error function. The principle of the variational methods has

been proven to be the equivalent integral of the differential equations and boundary conditions in mathematics. If the finite element conforms to the convergence criteria, the final approximate solution of the FEM converges to the exact solution of the original mathematical model [32]. The Duncan EB model is the most widely used nonlinear elastic constitutive model in the FEM analysis of soil structure [33,34]. In particular, we analysed the stress–strain characteristics of the dam in a 3-D FEM model to solve for the retrieved displacements (Figure 7). We defined the subdomain setting of the FEM model using the available geological and structural information. The process and the reservoir water filling were simulated in the analysis (Figure 8).

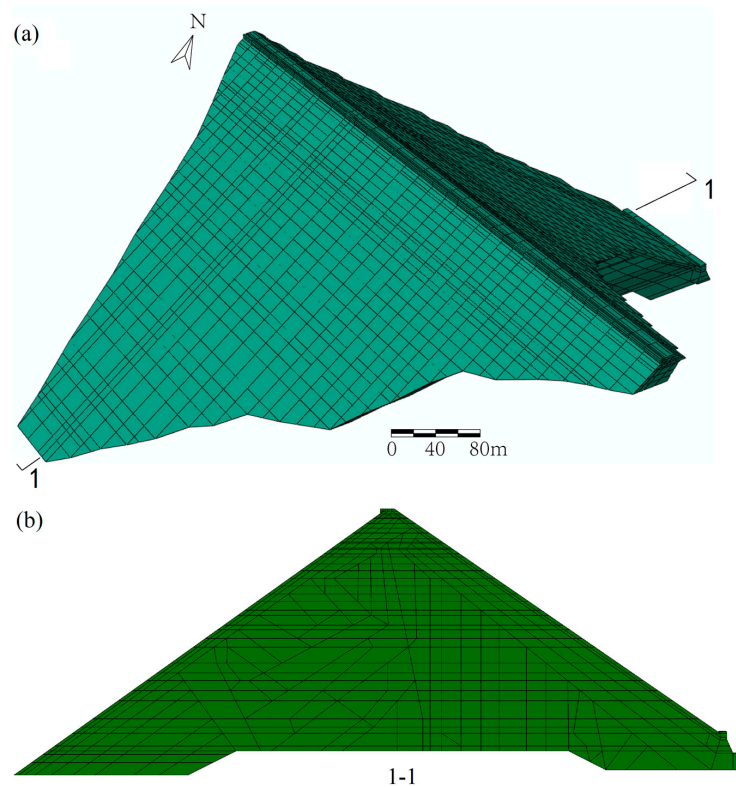


Figure 7. The 3D FEM mesh of the Shuibuya CFRD: (a) 3D FEM mesh, 1-1 is the biggest cross section of the SBY dam (0 + 212 m); and (b) 2D FEM mesh of the cross section of the 1-1 (0 + 212 m).

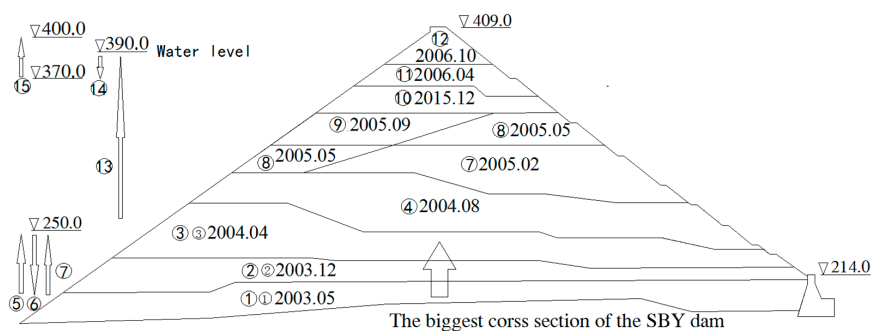


Figure 8. The process of construction and reservoir water filling. The numbers indicate the step of the dam construction and reservoir filling.

Due to its simplicity and the explicit physical meaning of its input parameters, the constitutive model proposed by Duncan has been widely used in civil engineering, especially for rockfill dams in China [33,34]. It can be described as follows:

$$E_t = K p_a \left(\frac{\sigma_3}{p_a}\right)^n [1 - S_L R_f]^2, E_{ur} = K_{ur} p_a \left(\frac{\sigma_3}{p_a}\right)^n$$

$$S_L = \frac{(1 - \sin\varphi)(\sigma_1 - \sigma_3)}{2c \cos\varphi + 2\sigma_3 \sin\varphi}, B_t = K_b p_a \left(\frac{\sigma_3}{p_a}\right)^m$$
(3)

where E_t is the tangent modulus, K is the modulus number, p_a is the atmospheric pressure, and σ_3 is the minor principal stress. n and R_f are the exponent and failure ratio, respectively. $\varphi = \varphi_0 - \Delta\varphi \lg(\sigma_3/p_a)$ is the internal friction angle, and c is the cohesive strength. σ_1 and σ_3 are the major and minor principal stresses, respectively. B_t is the bulk modulus. The rockfill of the dam has obvious creep characteristics. In this paper, the Merchant five-parameter creep model is used to describe the creep behaviour of rockfill materials [35].

$$\varepsilon_t = \varepsilon_f (1 - e^{-\alpha t}), \varepsilon_{sf} = d \left(\frac{S_L}{1 - S_L}\right)$$

$$\varepsilon_{vf} = b \left(\frac{\sigma_3}{p_a}\right)^{m_c} + \beta S$$
(4)

where ε_t is the creep strain, ε_f is the limit of the creep strain, α is a coefficient related to the creep strain rate, ε_{sf} is the limit of shear creep strain, and d, b, m_c and β are the creep parameters.

4.1.2. The Response Surface Method

Because of the complexity of engineering problems, the implementation of back-analysis is often time-consuming for a large number of the finite element analyses. In this study, the RSM with strong nonlinear mapping ability, is used to simulate the relationship between the parameter sets and the displacement of the monitoring points [4].

Twenty-seven parameter sets are generated using the orthogonal algorithms. Then, the FEM program that takes the static and creep properties of material into account is adopted to calculate the displacement at different monitoring points. The process of construction and reservoir water filling are simulated in the FEM analysis as show in Figure 8. In Li’s [4] study, the RSM considers only the static displacement of the rockfill. In this paper, the creep displacement is also taken into consideration. The RSM is given as follows:

$$S_k(\bar{x}) = a + \sum_{i=1}^N b_i \bar{x}_i + \sum_{i=1}^N c_i \bar{x}_i^2 + \sum_{j=1}^M d_j \bar{y}_j + \sum_{j=1}^M f_j e^{\bar{y}_j}$$
(5)

where \bar{x}_i and \bar{y}_j are the static and creep parameters to be identified, respectively. N and M are the numbers of the static and creep parameters, respectively a, b_i, c_i, d_j and f_j are the coefficients of the RSM to be identified. \bar{x}_i and \bar{y}_j can be calculated as follows:

$$\bar{x} = \left\{ \overline{\varphi_0}, \overline{\Delta\varphi}, \overline{k}, \overline{n}, \overline{R_f}, \overline{K_b} \right\}^T$$

$$\left. \begin{aligned} \overline{\varphi_0} &= \frac{\varphi_0}{\varphi_{01}}, \overline{\Delta\varphi} = \frac{\Delta\varphi}{\Delta\varphi_1}, \overline{k} = \frac{k}{k_1}; \\ \overline{n} &= \frac{n}{n_1}, \overline{R_f} = \frac{R_f}{R_{f1}}, \overline{K_b} = \frac{K_b}{K_{b1}} \end{aligned} \right\}$$
(6)

$$\bar{y} = \left\{ \overline{\alpha}, \overline{b}, \overline{m_c}, \overline{\beta}, \overline{d} \right\}^T$$

$$\left. \begin{aligned} \overline{\alpha} &= \frac{\alpha}{\alpha_1}, \overline{b} = \frac{b}{b_1}, \overline{m_c} = \frac{m_c}{m_{c1}}, \\ \overline{\beta} &= \frac{\beta}{\beta_1}, \overline{d} = \frac{d}{d_1} \end{aligned} \right\}$$
(7)

where $\varphi_{01}, \Delta\varphi_1, k_1, n_1, R_{f1}$ and K_{b1} are the values of the Duncan EB model parameters obtained from the laboratory; $\varphi_0, \Delta\varphi, k, n, R_f$ and K_b are the values after zooming in; $a_1, b_1, m_{c1}, \beta_1$ and d_1 are the values of the Merchant creep model parameters obtained from the laboratory; and a, b, m_c, β and d are the values after zooming in.

Then, the results of strain-stress analysis are used to calculate the coefficients of the RSM of every monitoring point using Equation (6). The RSM can simulate the relationship between the parameter set and the displacement of every monitoring point.

$$\left. \begin{aligned}
 S_1^1(\bar{x}) &= S(\bar{x}_1, \bar{x}_2, \dots, \bar{x}_M) \\
 S_1^2(\bar{x}) &= S(\bar{x}_1 + d\bar{x}_1, \bar{x}_2, \dots, \bar{x}_M) \\
 S_1^3(\bar{x}) &= S(\bar{x}_1 - d\bar{x}_1, \bar{x}_2, \dots, \bar{x}_M) \\
 &\dots\dots \\
 S_1^{26}(\bar{x}) &= S(\bar{x}_1, \bar{x}_2, \dots, \bar{x}_M + d\bar{x}_M) \\
 S_1^{27}(\bar{x}) &= S(\bar{x}_1, \bar{x}_2, \dots, \bar{x}_M - d\bar{x}_M)
 \end{aligned} \right\} \tag{8}$$

4.1.3. The Modified Genetic Algorithm

The parameter back-analysis of rockfill dams can be abstracted as an optimization problem in mathematics. The GAs proposed by Hollandin 1975 [36] have proven to be powerful for solving optimization problems. In this paper, a modified GA with global convergence is used to find the optimized parameter set of the objective function.

In GAs, the diversity of the population and the disproportionation between exploitation and exploration is conditioned by the crossover operator, which also influences the speed of convergence and determines the global convergence of the algorithm. The crossover operator is a basic operation with great importance. However, in the crossover operation of the traditional GA, the crossover points and the gene fragments are selected with randomness and blindness. It is difficult to generate new individuals when the selected gene fragments are highly similar to each other, that is, traditional crossover is not very effective in producing new generations that have great differences with their parents. This crossover operation is invalid and may decrease the diversity of the population.

Inspired by genetic engineering and the cloning of superior genes, a novel genetic crossover operator based on the sum of differences in gene fragments (SoDX) is proposed. The fragments' crossing probabilities are first evaluated based on the differences. The gene fragments are then selected and exchanged according to the crossing probability. This process can reduce inbreeding and the possibility of invalid crossover operations. A new GA code named SoDX-NUM was implemented in MATLAB by combining the crossover operator SoDX and the non-uniform mutation (NUM).

4.2. The Back-Analysis Results and the Argumentation

In this paper, six monitoring points (WS06–WS11) from levelling and InSAR with high precision and large displacement are used to invert the parameters. Using the displacement back-analysis method proposed in this paper, the identified model parameters set of rockfill based on the levelling and InSAR is determined, as shown in Table 1. Identified 1# and Identified 2# present the back-analysis results based on the levelling and InSAR monitoring results, respectively. K_1, n_1, K_{b1} and m_1 are the parameters of the Duncan EB model in the first material zone of the rockfill dam. K_2, n_2, K_{b2} and m_2 are the parameters of the Duncan EB model in the second material zone of the rockfill dam. a, b, m_c, β and d are the parameters of the creep constitutive model of the rockfill.

Table 1. The identified parameters using the back-analysis method based on the levelling and InSAR results.

Parameters	K_1	n_1	K_{b1}	m_1	K_2	n_2	K_{b2}	m_2	a	b (%)	m_c	β (%)	d (%)
Experimental	1100	0.35	600	0.1	850	0.25	400	0.05	0.009	0.0098	1.1338	0.64	0.21
Identified 1#	876	0.284	512	0.115	967	0.203	320	0.0579	0.00069	0.0113	1.334	0.77	0.168
Identified 2#	958	0.31	550	0.10	816	0.225	375	0.05	0.0007	0.0088	0.907	0.512	0.17

Identified 1# and Identified 2# are the back-analysis results of the levelling and InSAR, respectively.

Using the identified parameter sets of Identified 1# and Identified 2#, the FEM analysis is implemented. In the analysis, the process of dam construction and the water filling are simulated. The results are shown in the Figure 9, including the settlement process of the levelling, the identified parameter set based on the levelling, and the identified parameter set based on InSAR.

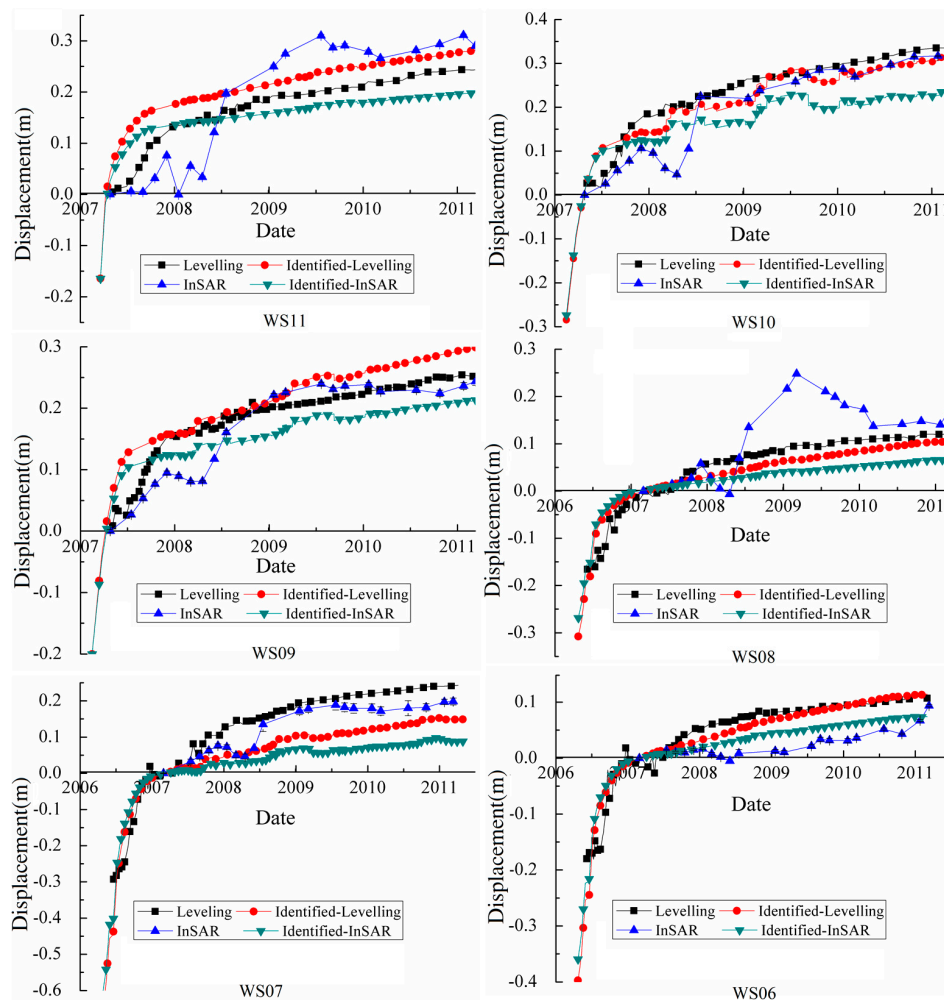


Figure 9. The displacement for WS05–WS11 based on the levelling, levelling-identified, InSAR and InSAR-identified parameters.

The traditional back-analysis methods use internal monitoring data. In this study, the external monitoring results are used as the objective function to perform the back-analysis. The correlation of the levelling monitoring data and the computed results based on Identified 1# of the six points are 0.97, 0.96, 0.95, 0.96, 0.93 and 0.96. This suggests that the displacement pattern of the calculated results using the identified parameters set of levelling agree well with the observed levelling values, which indicates that the identified parameters, in general, satisfactorily reflect the displacement properties of the dam. The external monitoring data could be used to map the displacement properties of the dam. The InSAR results are also used to perform the parameters back-analysis. Figure 9 shows the computed settlement based on Identified 2# and the InSAR monitoring results. They have similar magnitude and distribution.

The back-analysis results based on levelling data and InSAR monitoring data are also compared. The displacement from 28 February 2007 to 11 March 2011 is shown in Figure 10a,b and the higher elevation, the greater the displacement increment. In addition, the differences and the correlation are shown in Figure 10c,d. The computed displacement of the two identified parameter sets have little

difference with each other (Figure 10c). The correlation of the displacement results generated from InSAR and levelling is 0.99 (Figure 10d). The displacement in the middle of the dam is greater than at the two sides. The greatest total displacement increment of the FEM computed result is 0.467 m, which is similar to the InSAR results. It also shows that the computed results and the results of InSAR have similar displacement increment distributions, and the displacement computed using the parameters Identified 2# has similar magnitude and distribution as the InSAR monitoring results.

Combining the time series analysis and back-analysis, it can be concluded that InSAR technology can be used as a supplement for the traditional monitoring method to monitor high dams and can also be used as a method to invert the parameters of the dam.

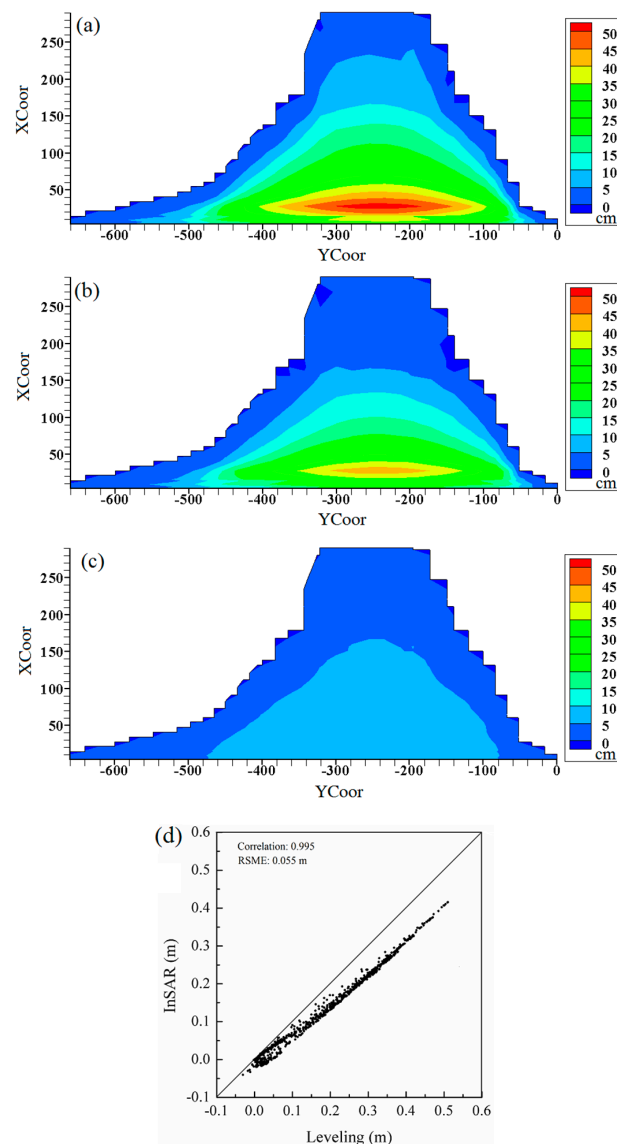


Figure 10. Comparison of the displacement increment from 28 February 2007 to 11 March 2011: (a) Vertical displacement computed by the FEM model and the identified parameters based on levelling (1#); (b) Vertical displacement computed by FEM model and the identified parameters based on the InSAR results (2#); (c) The displacement difference between (a) and (b); (d) The Correlation between InSAR and levelling measurements, and black line in is a 1:1 line. XCoord means the direction of the river flow, YCoord means the direction from the left bank to the right bank. The units of X and Y-axes are in meters.

4.3. Settlement Prediction for the SBY Dam

The FEM model, the constitutive model and the back-analysis results can accurately represent the time-dependent displacement of the SBY dam. To study the post-construction settlement of the SBY dam, further FEM analysis is performed to predict the dam displacement using the parameters identified based on the InSAR results. The settlement contours of cross-section 0 + 212 m for 30 December 2020 are given in Figure 11. The maximum settlement is 2.332 m, approximately 1% of the dam height. The maximum settlement occurs in the centre of the dam body, whereas the settlement of upstream (left) and downstream (right) of the dam is smaller (<40 cm), and the settlement increases towards the centre. The biggest settlement located at the core of the dam mainly because of following two reasons: (1) Because of the gravity of rockfill in different layers and intervals between the different stages of concrete-face construction, most settlement of the lower layer filled rockfill is happened when the upper layer rockfill is completed on the dam. The SBY dam has different material zones, which are shown in Figure 2a). The rockfill is gradually filled according to layer during the construction period. For example, the first stage of concrete-face is constructed after the rockfill of the dam was decreased six or nine months, then the second stage concrete-face and the third concrete face. (2) Because of arching effects caused by different settlement rate of the dam body in the parallel and perpendicular direction of the river. In the direction of perpendicular to the river, due to the V-shaped valley, the arching effect is raised when the settlement rate of the central rockfill is faster than the two sides of the rockfill, which contributes an uplift force to the central rockfill. While in the direction of parallel to the river flow, the other arching effect is caused because of the settlement rate in the central is faster than the upstream and downstream of the dam, which also produces an uplift force to the central rockfill. Therefore, the maximum displacement occurs in the centre of the dam.

The settlement increments from 28 February 2007 to 11 March 2011 and to 30 December 2020 are given in Figure 12a,b, respectively, and their corresponding difference is shown in Figure 12c. Figure 12a,b shows that the displacement increment is approximately 60 cm at the dam crest, and the upstream is greater than the downstream. From the Figure 12c, it can be observed that the settlement at the top and upstream (left) is much greater than that downstream (right) from the dam. This difference is due to water filling; the load of the upstream (left) of the dam is greater than the downstream load (right). The settlement is smaller than 10 cm from 11 March 2011 to 30 December 2020 and is approximately 60 cm from 2007 to 2011. This suggests that the displacement increases rapidly in the early reservoir period, and the settlement trends toward stability in the later operation period. The displacement consists of instantaneous and creep displacement. Most of the later settlement is creep displacement, and the basic characteristic of creep displacement is that it decreases gradually with the time. These results agree with the displacement characteristics of the dam.

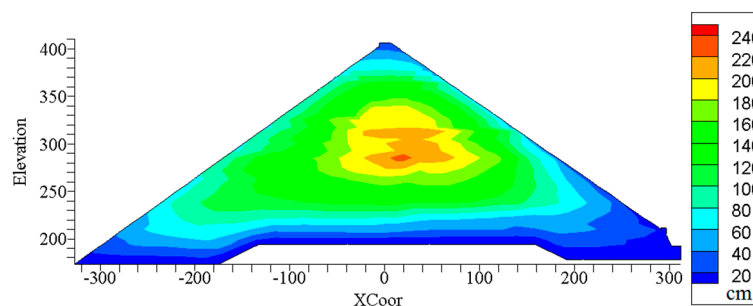


Figure 11. The settlement contours of cross-section 0 + 212 m for 30 December 2020. XCoord means the direction of the river flow. The units of X and Y-axes are in meters.

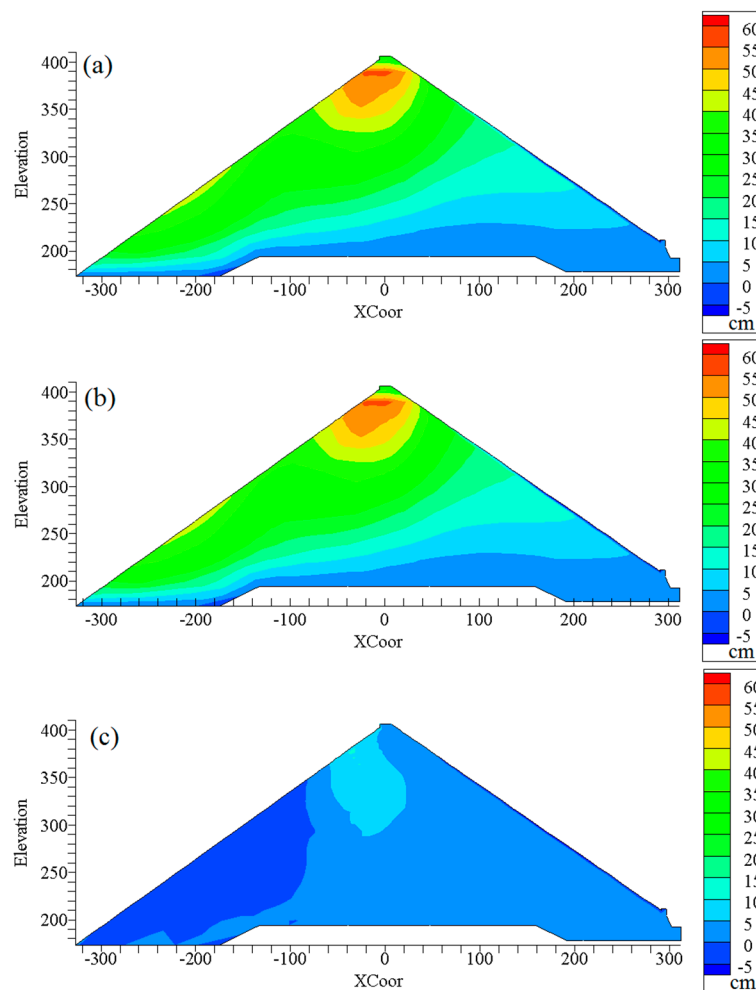


Figure 12. The settlement increment contours of cross-section 0 + 212 m: (a) The settlement increment from 28 February 2007 to 11 March 2011; (b) The settlement increment from 28 February 2007 to 30 December 2020; and (c) The settlement increment from 11 March 2011 to 30 December 2020. XCoord means the direction of the river flow. The units of X and Y-axes are in meters.

5. Discussions

In our previous study, the InSAR technique was used to investigate the displacement of the SBY Dam, and the reliability was compared with levelling measurements. The results provide confidence that the InSAR time series is a useful tool for CFRD displacement monitoring [16]. In this study, to further investigate the inside features of the SBY dam, the FEM, RSM and GA are used to identify the mechanical parameters of the rockfill, and then the associated displacement time series and settlement is simulated. The Duncan EB model is the most widely used nonlinear elastic constitutive model in the numerical analysis of soil structure. The triaxial shear tests show that the Duncan EB model is capable of simulating the stress–strain relationship of rockfill materials. The computed results of the previous rockfill dams and the in situ monitoring data have proven the precision of the Duncan EB model [4,9,33].

To examine the stability and security of the CFRD, the physical parameters of the rockfill are pre-requisite for settlement prediction. Due to the size effect, sample disturbance and the impact of random sampling, it is difficult to guarantee the represent activeness of the experiment results. Parameter back-analysis is an efficient way to identify parameters. In this paper, the levelling and InSAR measurement results are used to perform the parameter back-analysis. The results show that the trend, the magnitude and the distribution of the displacement of the SBY Dam downstream surface

agree well with each other (Figures 9 and 10). The high correlation of 0.995 and a low RMSE of 0.055 m between the results based on InSAR and the results based on the levelling measurements suggest that the back-analysis based on the InSAR technique is a reliable way to identify the parameters of a rockfill dam. The low RMSE indicates that the back-analysis method is accurate and useful for obtaining the mechanical parameters of the dam. The internal ground monitoring data continues to 16 March 2012. The maximum settlement from the ground monitoring data is 2.536 m, and it is 2.156 m based on the rockfill parameters from the InSAR results, which confirms that the combination of InSAR measurement and the FEM back-analysis is a reliable way to identify the parameters and to predict the displacement of rockfill dams. The results also suggest the stability and security of the SBY CFRD between 2007 and 2020.

The density and coverage of the InSAR measurement can be much higher than conventional survey methods, such as levelling and GPS. In addition to the displacement of the dam body, the stability of the surroundings of the dam can be determined by the InSAR method. This is important because the geologic stability of a dam's surroundings has a great impact on its behaviour. Moreover, many high CFRDs will be built in the northwest of China, where earthquake frequently occur; thus, accurate monitoring is a guarantee of their security. Compared to conventional measurements, the InSAR is an efficient supplement technology to the traditional methods in the long term.

6. Conclusions

The physical parameters of the SBY dam are identified using the proposed back-analysis method by combining the FEM model and the InSAR time series results. The displacement results using the identified parameters agree well with the observed levelling values in both magnitude and distribution. The settlement prediction of the SBY Dam is performed using the identified parameters, and the maximum settlement is 2.332 m, approximately 1% of the dam height. The settlement of the SBY Dam becomes stable in the later operation period. The back-analysis method using the external monitoring data from InSAR can record the displacement properties of the dam. The InSAR technology can be used as supplement for the traditional monitoring methods to monitor high dams and can also be used to invert the parameters of the dam.

Acknowledgments: This research was supported by the National Natural Science Foundation of China (No. 1322905) and China Postdoctoral Science Funding (2015M570666). We also acknowledge Zhenhong Li for providing the InSAR + AEM InSAR time series package.

Author Contributions: Wei Zhou, Shaolin Li, Zhiwei Zhou, and Xiaolin Chang developed the main idea of this study, and Wei Zhou guided the project. Shaolin Li and Wei Zhou contributed to the ground monitoring data analysis, parameters back-analysis and FEM analysis. Zhiwei Zhou performed the ALOS PALSAR data interferometry processing and analysis. Zhiwei Zhou, Shaolin Li and Wei Zhou contributed to discussion of the final results and writing the manuscript.

Conflicts of Interest: The authors declare no conflict of interest.

References

1. Wei, Z.; Xiaolin, C.; Chuangbing, Z.; Xinghong, L. Creep analysis of high concrete-faced rockfill dam. *Int. J. Numer. Methods Biomed. Eng.* **2010**, *26*, 1477–1492. [[CrossRef](#)]
2. Hua, J.; Zhou, W.; Chang, X.; Zhou, C. Study of scale effect on stress and deformation of rockfill. *Chin. J. Rock Mech. Eng.* **2010**, *2*, 328–335.
3. Wu, Y.; Yuan, H.; Zhang, B.; Zhang, Z.; Yu, Y. Displacement-based back-analysis of the model parameters of the nuozhadu high earth-rockfill dam. *Sci. World J.* **2014**, *2014*, 292450. [[CrossRef](#)] [[PubMed](#)]
4. Li, S.J.; Zhang, J.; Liang, J.Q.; Sun, Z.X. Parameter inversion of nonlinear constitutive model of rockfill materials using observed deformations after dam construction. *Rock Soil Mech.* **2014**, *35*, 61–67.
5. Jing, L. A review of techniques, advances and outstanding issues in numerical modelling for rock mechanics and rock engineering. *Int. J. Rock Mech. Min. Sci.* **2003**, *40*, 283–353. [[CrossRef](#)]
6. Li, Z.; Li, J.; Zheng, S.; Wu, Q. Several measures for improving hydraulic overflow settlement gauge. *Hydropower Autom. Dam Monit.* **2010**, *6*, 31–33.

7. Han, J.; Zhang, C. Experimental research on the installation of pipe-type settlement gauge in nuozhadu hydropower station. *Water Power* **2012**, *38*, 96–99.
8. Liu, G.; Li, Z.; Li, X.; Wang, J. Experimental analysis of horizontal displacement monitoring device with long pipeline tensile. *Hydropower Autom. Dam Monit.* **2012**, *4*, 53–56.
9. Yu, Y.; Zhang, B.; Yuan, H. An intelligent displacement back-analysis method for earth-rockfill dams. *Comput. Geotech.* **2007**, *34*, 423–434. [[CrossRef](#)]
10. Zhao, H.-B.; Yin, S. Geomechanical parameters identification by particle swarm optimization and support vector machine. *Appl. Math. Model.* **2009**, *33*, 3997–4012. [[CrossRef](#)]
11. Zheng, D.; Cheng, L.; Bao, T.; Lv, B. Integrated parameter inversion analysis method of a CFRD based on multi-output support vector machines and the clonal selection algorithm. *Comput. Geotech.* **2013**, *47*, 68–77. [[CrossRef](#)]
12. Di Martire, D.; Iglesias, R.; Monells, D.; Centolanza, G.; Sica, S.; Ramondini, M.; Pagano, L.; Mallorquí, J.J.; Calcaterra, D. Comparison between differential SAR interferometry and ground measurements data in the displacement monitoring of the earth-dam of Conza della Campania (Italy). *Remote Sens. Environ.* **2014**, *148*, 58–69. [[CrossRef](#)]
13. Wang, T.; Perissin, D.; Rocca, F.; Liao, M.-S. Three gorges dam stability monitoring with time-series InSAR image analysis. *Sci. China Earth Sci.* **2011**, *54*, 720–732. [[CrossRef](#)]
14. Lazecký, M.; Perissin, D.; Zhi, W.; Ling, L.; Yu, Q. Observing dam's movements with spaceborne SAR interferometry. In *Engineering Geology for Society and Territory*; Lollino, G., Manconi, A., Guzzetti, F., Culshaw, M., Bobrowsky, P., Luino, F., Eds.; Springer: Berlin/Heidelberg, Germany, 2015; Volume 5, pp. 131–136.
15. Voege, M.; Frauenfelder, R.; Larsen, Y. Displacement monitoring at Svartevatn dam with interferometric SAR. In Proceedings of the 2012 IEEE International Geoscience and Remote Sensing Symposium (IGARSS), Munich, Germany, 22–27 July 2012; pp. 3895–3898.
16. Zhou, W.; Li, S.; Zhou, Z.; Chang, X. Remote sensing of deformation of a high concrete-faced rockfill dam using InSAR: A study of the Shuibuya dam, China. *Remote Sens.* **2016**, *8*, 255. [[CrossRef](#)]
17. Werner, C.; Wegmüller, U.; Strozzi, T.; Wiesmann, A. Gamma SAR and interferometric processing software. In Proceedings of the ERS-Envisat Symposium, Gothenburg, Sweden, 16–20 October 2000; p. 1620.
18. Farr, T.G.; Rosen, P.A.; Caro, E.; Crippen, R.; Duren, R.; Hensley, S.; Kobrick, M.; Paller, M.; Rodriguez, E.; Roth, L.; et al. The shuttle radar topography mission. *Rev. Geophys.* **2007**, *45*, RG2004. [[CrossRef](#)]
19. Eineder, M.; Hubig, M.; Milcke, B. Unwrapping large interferograms using the minimum cost flow algorithm. In Proceedings of the 1998 Geoscience and Remote Sensing Symposium Proceedings, Seattle, WA, USA, 6–10 July 1998; pp. 83–87.
20. Hanssen, R.F. *Radar Interferometry: Data Interpretation and Error Analysis*; Kluwer Academic Publishers: Dordrecht, The Netherlands, 2001.
21. Ferretti, A.; Prati, C.; Rocca, F. Permanent scatterers in SAR interferometry. *IEEE Trans. Geosci. Remote Sens.* **2001**, *39*, 8–20. [[CrossRef](#)]
22. Berardino, P.; Fornaro, G.; Lanari, R.; Sansosti, E. A new algorithm for surface deformation monitoring based on small baseline differential SAR interferograms. *IEEE Trans. Geosci. Remote Sens.* **2002**, *40*, 2375–2383. [[CrossRef](#)]
23. Hooper, A.; Segall, P.; Zebker, H. Persistent scatterer interferometric synthetic aperture radar for crustal deformation analysis, with application to Volcán Alcedo, Galápagos. *J. Geophys. Res.* **2007**, *112*, B07407. [[CrossRef](#)]
24. Doin, M.-P.; Guillaso, S.; Jolivet, R.; Lasserre, C.; Lodge, F.; Ducret, G.; Grandin, R. Presentation of the small-baseline NSBAS processing chain on a case example: The Etna deformation monitoring from 2003 to 2010 using Envisat data. In Proceedings of the Fringe Symposium, Frascati, Italy, 19–23 September 2011; pp. 303–304.
25. Ferretti, A.; Fumagalli, A.; Novali, F.; Prati, C.; Rocca, F.; Rucci, A. A new algorithm for processing interferometric data-stacks: Squeasar. *IEEE Trans. Geosci. Remote Sens.* **2011**, *49*, 1–11. [[CrossRef](#)]
26. Li, Z.; Fielding, E.J.; Cross, P. Integration of InSAR time-series analysis and water-vapor correction for mapping postseismic motion after the 2003 Bam (Iran) earthquake. *IEEE Trans. Geosci. Remote Sens.* **2009**, *47*, 3220–3230.

27. Zhang, L.; Ding, X.; Lu, Z. Ground settlement monitoring based on temporarily coherent points between two SAR acquisitions. *ISPRS J. Photogramm. Remote Sens.* **2011**, *66*, 146–152. [[CrossRef](#)]
28. Sowter, A.; Bateson, L.; Strange, P.; Ambrose, K.; Syafiudin, M.F. DInSAR estimation of land motion using intermittent coherence with application to the South Derbyshire and Leicestershire coalfields. *Remote Sens. Lett.* **2013**, *4*, 979–987. [[CrossRef](#)]
29. Li, Z.; Fielding, E.J.; Cross, P.; Muller, J.-P. Interferometric synthetic aperture radar atmospheric correction: GPS topography-dependent turbulence model. *J. Geophys. Res. Solid Earth* **2006**, *111*, B02404. [[CrossRef](#)]
30. Williams, S.; Bock, Y.; Fang, P. Integrated satellite interferometry: Tropospheric noise, GPS estimates and implications for interferometric synthetic aperture radar products. *J. Geophys. Res. Solid Earth* **1998**, *103*, 27051–27067. [[CrossRef](#)]
31. Hammond, W.C.; Blewitt, G.; Li, Z.; Plag, H.P.; Kreemer, C. Contemporary uplift of the Sierra Nevada, western United States, from GPS and InSAR measurements. *Geology* **2012**, *40*, 667–670. [[CrossRef](#)]
32. Zienkiewicz, O.C.; Taylor, R.L.; Zienkiewicz, O.C.; Taylor, R.L. *The Finite Element Method*; McGraw-Hill: London, UK, 1977; Volume 3.
33. Duncan, J.M.; Chang, C.-Y. Nonlinear analysis of stress and strain in soils. *J. Soil Mech. Found. Div.* **1970**, *96*, 1629–1653.
34. Duncan, J.M.; Wong, K.S.; Mabry, P. Strength, stress–strain and bulk modulus parameters for finite element analyses of stresses and movements in soil masses. In *Geotechnical Engineering*; University of California: Berkeley, CA, USA, 1980.
35. Wang, G.-Q.; Yu, T.; Li, Y.-H.; Li, G.-Y. Creep deformation of 300 m-high earth core rockfill dam. *Chin. J. Geotech. Eng.* **2014**, *36*, 140–145.
36. Holland, J.H. *Adaptation in Natural and Artificial Systems. An Introductory Analysis with Application to Biology, Control, and Artificial Intelligence*; University of Michigan Press: Ann Arbor, MI, USA, 1975.



© 2016 by the authors; licensee MDPI, Basel, Switzerland. This article is an open access article distributed under the terms and conditions of the Creative Commons Attribution (CC-BY) license (<http://creativecommons.org/licenses/by/4.0/>).